2013 IEEE International Conference on Robotics and Automation (ICRA)
Karlsruhe, Germany, May 6-10, 2013

Extended Gait Equation for Sidewinding

Chaohui Gong, Matthew J. Travers, Xiaozhou Fu and Howie Choset
{chaohuig, mtravers, xf choset}@cmu.edu

Abstract— **Sidewinding is an efficient translational gait used by biological snakes to locomote over flat ground. Prior work has identified the fact that it is possible to steer the moving direction of sidewinding. The previously proposed *virtual tread* model reveals the working principal of sidewinding from a geometric point of view. Unfortunately, the implementation of the virtual tread model relied on a computationally expensive numerical fitting algorithm that impeded online applications. Motivated by this limitation, in this work we propose a novel approach to develop analytical expressions for snake robot gaits based on the study of the corresponding geometric model. This approach is rooted in the identification of dominant frequency components afforded by the two-dimensional Fast Fourier Transformation (FFT). Applying this method to the virtual tread model for conical sidewinding, we derive an analytical expression between the parameters that describe the gait's motion and the *turning radius* of the system moving in the world. This analytical expression, which we call the extended gait equation, is verified by experimental results.**

I. Introduction

Snake robots are a class of hyper-redundant mechanism capable of executing versatile gaits, cyclic changes in shape, through complex environments. A variety of different gait design methods for these hyper-redundant mechanisms have been developed within the snake robot community. For example, the gait equation identified in [1] expresses joint angles as a function of joint index and time. The gait equation provides a reduced analytical representation that directly evaluates to joint position and velocity commands. Gait equations are thus ideal for real-time implementations of snake motions on discrete mechanisms. However, deriving new gaits using the gait equation can be quite difficult, as the gait parameters do not necessarily have any intuitive physical interpretation.

As an alternative, the *backbone curve* approach [2] creates a gait by first capturing the macroscopic shape of the snake robot with a backbone curve and then animates the curve to execute a gait. Backbone curves are geometrically intuitive but by themselves do not directly generate control inputs. In prior work, we used a *chain fitting* [3] algorithm to overcome this limitation; joint angles are generated by numerically fitting the discrete segments of the robot onto the desired backbone curve. To represent a gait, a sequence of backbone curves are fit and the results stored in a numerical lookup table. The drawback of this approach is that a new lookup table must be calculated for any variation resulting in a new gait. The process of generating a new lookup table is computationally expensive, and must be done offline. In addition, the inherently discrete representations of gaits in terms of lookup tables impede smooth transitions between gaits.

The first main contribution of this paper is the identification of a gait design approach which leverages the benefits of both gait equations and backbone curves. We show that we are able to derive analytical gait representations which encode the physical geometry of the system embedded in the world. In order to illustrate the benefits of this approach, we select the sidewinding gait as a canonical example. Sidewinding is an efficient gait [1] widely adopted by both biological snakes as well as snake-like robots locomoting on flat terrain. During execution of a gait cycle, sidewinders generate net displacement by pushing against the ground with a limited set of body contact regions. In addition to locomotion on flat ground, sidewinding is also known for its wide adaptability to rocky, loose, and slippery environments.

In [4], the virtual tread model, in which the *backbone curve* of sidewinding is abstracted as a moving tread on the surface of a rolling cylinder, was proposed. In this previous work, the cylinder to which the backbone curve was *fit* was referred to as the core geometry for the sidewinding gait. This helical tread model closely corresponds to the shape produced by snake-like robots executing sinusoid-based sidewinding, as described in [1], [5]–[8]. In our conical sidewinding work [9], we generalized the tread model by tapering the core geometry into a cone to generate turning motion while sidewinding.

In this work, we derive an analytical formulation for conical sidewinding, called the extended gait equation. The second main contribution of this work is the single parameter representation of sidewinding. It is shown that the extended gait equation can be used to provide continuous and precise control over the turning radius of the robot while locomoting.

This paper is organized as follows: First, we present necessary background information which is extensively used in the development of the extended gait equation. Second, we identify the dominant frequency components of the *wave surface* of conical sidewinding by using the 2 dimensional Fast Fourier Transformation (FFT). This is followed by the derivation of the extended gait equation. Finally, experimental results supporting our theoretical findings are presented.

II. Background

Our research group, as well as others, have developed a variety of equations to model the motion of a gait in a snake robot. With our gait model, we have been able to vary the parameters to derive a variety of gaits, but this approach

978-1-4673-5642-8/13/$31.00 ©2013 IEEE

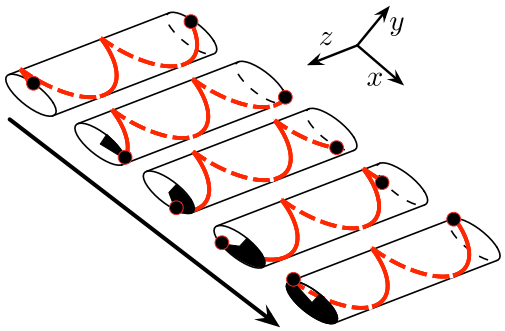

Fig. 1: The helical *backbone curve* (red) of sidewinding rolls forward with the evolution of time. This figure shows the shape of the *backbone curves* at evenly sampled *keyframes* in one gait period.

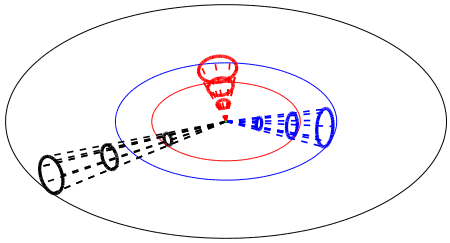

Fig. 2: The *backbone curve* (red) of a sidewinding snake resembles a conical helix wrapping around the surface of a virtual cone. While the cone is rolling on the ground, the snake's heading direction is instantaneously governed by the radius of the cone.

tended to be unintuitive. Therefore, we considered an approach that allowed us to manipulate the backbone curve to generate gaits; we termed this approach the keyframe method because we considered snap shots of the backbone curve while executing a gait and then fit a surface, called a wave surface through the key frames. We were able to use this method to generate a gait equation for sidewinding, but this approach, in general, did not generate parameters that fit into our existing gait equation. In other words, there were gaits that our gait equation did not capture. In this paper, we seek an analytic means to capture such gaits, including conical sidewinding. In order to do so, we rely on a shape stable body frame, called *virtual chassis*, as our reference frame to represent the configuration of the whole robotic system.

A. Gait Equation

An elegant way to express gaits for a snake robot is the gait equation, which expresses joint angles as a function of joint index and the phase of the gait cycle. The gait equation of linear translational sidewinding can be expressed as,

$$\alpha(n,t) = \begin{cases} \beta_{odd} + A\sin(\theta_{odd}) & \text{odd} \\ \beta_{even} + eA\sin(\theta_{even} + \delta) & \text{even} \end{cases} \quad (1)$$
$$\theta_{odd,even} = (\Omega_{odd,even} n + \omega_{odd,even} t),$$

where β, A, θ, e and δ are respectively angle offset, amplitude, phase, aspect ratio and phase shift. This gait equation compactly implements the joint movements [1], [7], which can be directly used as a control signal for the joint inputs. In addition, a gait equation provides an analytically parameterized smooth representation; the properties of the gait can continuously be adjusted by continuously varying the parameters.

B. Keyframe

The *backbone curve* representing a snake gait changes periodically over a gait cycle. It thus stands to reason that the joint angles of a snake robot fit to this changing *backbone curve* should also evolve periodically. In order to generate the joint angle inputs from a series of changing *backbone curves* over a gait cycle, the *keyframe* [3] approach was proposed. This method discretizes a gait cycle into evenly distributed time steps. At each time step, the shape of *backbone curve* is frozen , as illustrated in Fig. 1, and the joint angles of a snake robot approximating this curve are generated by a fitting algorithm. Considering the fact that our snake robot is an alternating chain of pitch and yaw joints, the fitting process is computationally burdensome; every step of the fitting algorithm effectively solves a constrained optimization. The constraints arise from the kinematic structure of the robot.

C. Sidewinding: The Virtual Tread Model

Prior researches in the study of the working mechanism of sidewinding include Mosauer's seminal work [10] on ophidian locomotion and the mathematical formulation for the *backbone curve* of sidewinding proposed by Burdick, Radford and Chirikjian [2]. Our 'virtual tread' model [4], [9] abstracts a sidewinding snake as a moving *backbone curve* wrapped around the surface of a virtual cone, hence called conical sidewinding. The robot moves along curved paths on the terrain by 'rolling' the virtual cone. Changing the taper of the virtual cone changes the turning radius of the robots path, as illustrated in Fig. 2.

D. Virtual Chassis

Because of the redundant property and complex shape changes of a snake robot during a gait, it is difficult to represent and measure the snake motion in an intuitive and meaningful way. To address this problem, we take a shape stable body frame, called *virtual chassis* [11], as our reference frame, which is independent of the current gait. Rather than rigidly attach a body frame onto one of the 16 links, the *virtual chassis* is defined by the overall body shape of the snake robot. The origin of the *virtual chassis* coincides with the center of mass (COM) of the snake robot, and the orientation is identified by continuously aligning it with the principal moments of inertia.

III. Dominant Components of Wave Surface

The attractive component of the wave equation is that it allows an arbitrary number of joints to be controlled by a low-dimensional, analytical, parameterized, and sinusoidal *basis* function. The limitation of (1) is that it is not immediately clear that it is adaptable for parameterizations of the full space of potentially interesting gaits. What is clear however, is that joint movement during gait execution is periodic. It is thus natural to choose sinusoids at different frequencies as

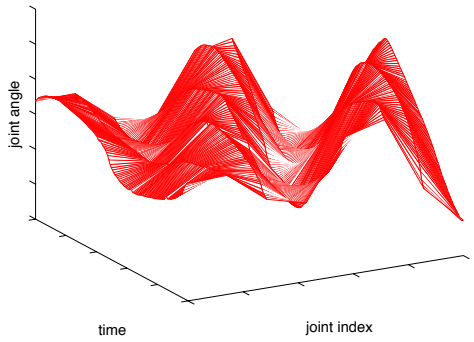

Fig. 3: *Wave surface* of conical sidewinding produced by the chain fitting algorithm. The amplitude of joint angle varies with time and joint index.

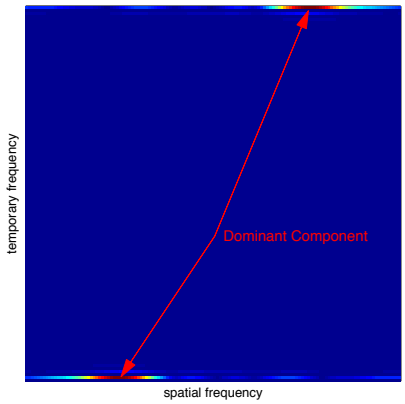

Fig. 4: Transforming the *wave surface* into the frequency domain provides a clear view of the composing frequency components in space and time. Red color denotes frequency components of high strength and blue area indicates low amplitudes. The presence of two strong area in the figure is due to the symmetric property of 2D FFT.

candidate function bases for a generalized gait parameterization. In this section, we proposed a novel approach aimed at identifying the dominant modes of parameterized-sinusoidal gait basis functions. The identification of dominant modes is accomplished via frequency component analysis of *wave surfaces* using the two-dimensional Fast Fourier Transformation (FFT).

A. Wave Surface

Wave surfaces provide a means of visualizing a collection individual joint movements throughout a gait period. In prior implementations, the joint angles were calculated by a fitting algorithm at evenly distributed *keyframes*, frames discretely separated in time. The *wave surface* representation offers a macroscopic view of the evolution of joint angles as a function of both joint index and time. Note that the 'continuous' wave surface shown in Fig. 3 is generated by interpolation of several keyframe fit solutions. Applying a 2D FFT to a discrete wave surface, it is possible to identify principal frequency components. Identification of the dominant frequency components makes it possible to derive

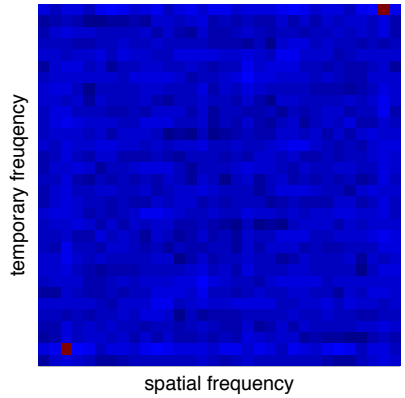

Fig. 5: This is the frequency strength plot of linear-translational sidewinding. Red color denotes frequency components of high strength and blue area indicates low amplitudes.

an extended gait equation which approximates the original *wave surface*.

B. Dominant Components

We apply the 2D FFT to the *wave surface* in Fig. 3 to extract the wave pattern and to identify the dominant frequency components of conical sidewinding. Fig. 4 shows the strength of frequency components at different spatial and temporary frequencies. It is clear in Fig. 4 that the main temporal frequency components have a very narrow bandwidth, while the strong spatial frequency components span a relatively wide range. In contrast, the dominant frequency components of linear-translational sidewinding has a narrow range in both time and space, which is shown in Fig. 5.

To supplement the missing spatial frequency components in Fig. 4, we propose to extend the original gait equation into a general form as follows,

$$\alpha(n,t) = \begin{cases} A(n)\sin(\theta_{odd}) & \text{odd} \\ eA(n)\sin(\theta_{even}+\delta) & \text{even} \end{cases} \quad (2)$$
$$\theta_{odd,even} = (\Omega_{odd,even}n + \omega_{odd,even}t),$$

where the amplitude $A(n)$ has been modified to be a function of joint index n, rather than a constant as it is in (1) (notice: $\beta = 0$ for sidewinding). The presence of this amplitude function $A(n)$ varies the distribution of dominant frequency components in Fig. 5, and one $A(n)$ which complements the aforementioned missing frequency components can be found.

IV. Extended Gait Equation

Having identified the general form of the extended gait equation, the remaining work is to recover the amplitude function $A(n)$.

A. Amplitude Function

Based on the observation that the amplitude of the wave pattern in Fig. 3 appears to increase linearly along the joint index axis, we make the assumption that the amplitude of the joint angles should monotonically increase along the body of

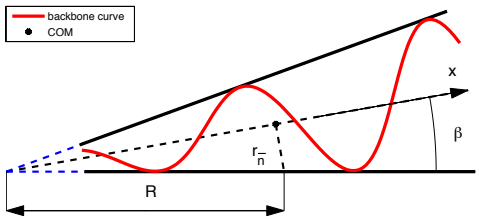

Fig. 6: A side view of conical sidewinding reveals the geometric relationship between the aperture β, turning radii R and the virtual cone's size $r_{\bar{n}}$, as described by the distance from the center of mass (COM) to the cone's surface. The *backbone curve* (red) spins around the central axis x.

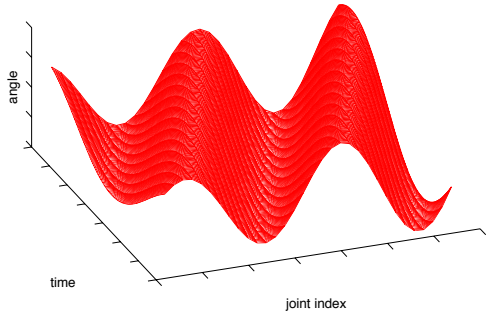

Fig. 7: This is the *wave surface* produced by substituting discrete time steps and joint indices into our extended gait equation. Strong similarity to the *wave surface* Fig. 3 generated by chain fitting algorithm is observed.

the snake robot. Fig. 6 provides a side view of the *backbone curve* of conical sidewinding, where the black lines are the edges of the virtual cone. The amplitude of the sinusoidal curve in this 2D view can be expressed as,

$$y(x) = ax, \tag{3}$$

where x is the central axis of the virtual cone. The slope a in (3) is related to aperture of the virtual cone β, by

$$a = \tan(\beta). \tag{4}$$

However, we notice the amplitude function $A(n)$ in the extended gait equation is parameterized as a function of joint index n or, equivalently, the length along the *backbone curve* s, which is the continuous equivalence to joint index. The shapes of sinusoids can be closely approaximated by serpenoid curves when the aperture β is close to zero. And, the relation between the length along the central axis x and the distance along a serpenoid curve s is established as,

$$x(s) = sJ_0(\theta) + \frac{4l}{\pi}\sum_{m=0}^{\infty} J_{2m}(\theta)\sin(m\pi\frac{s}{l}), \tag{5}$$

in which θ is the *winding angle*, $4l$ is the wave length of a serpenoid curve along x, as defined in [12], and $J_m(\theta)$ denotes a Bessel function of the first kind. As the aperture β varies in a small range, (5) can be approximated as,

$$x(s) = J_0(\bar{\theta})s, \tag{6}$$

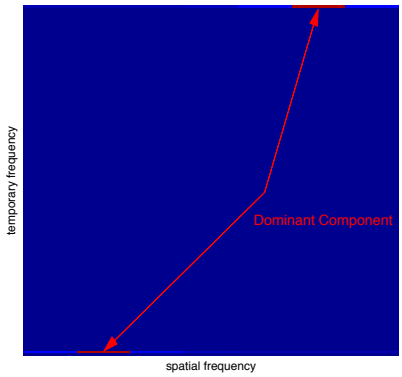

Fig. 8: The frequency strength plot of the *wave surface* of our extended gait equation. Red color denotes strong frequency components and blue means low amplitude.

where $\bar{\theta}$ is a constant. Consequently, by substituting (6) into (3), the amplitude $y(s)$ turns out to be a linear function of s,

$$y(s) = aJ_0(\bar{\theta})s \approx \frac{A(s)}{m}, \tag{7}$$

where m is a constant coefficient [12]. Inspired by this linear relation and based on the joint angle approximation proposed in [13], the amplitude function in the extended gait equation can be formulated as

$$A(n) = k(n - \bar{n}) + A_{\bar{n}}, \tag{8}$$

where $\bar{n}$ is the middle joint index and k is the slope which will be shown to determine the turning radius of the gait in Section IV-B. Fig. 7 and Fig. 8 respectively show the *wave surface* and frequency strength corresponding to the extended gait equation. The similarity between Fig. 7 and Fig. 3 indicates a close approximation of the extended gait equation to the *wave surface* which resulted from the *chain fitting* algorithm.

B. Control of Turning Radii

To meaningfully measure the displacement and distinguish the orientation of the snake robot, we take the shape-stable body frame, *virtual chassis* [11], as our reference. For sidewinding, the origin of *virtual chassis* frame is roughly located at the middle point of the bodies central axis, x, as depicted in Fig. 6. According to (8), the amplitude in the middle of the serpenoid curve is consistently commanded to be $A_{\bar{n}}$, as shown in Fig. 9. Hence, the perpendicular distance from the position of the origin of the virtual chassis frame to the surface of the virtual cone $r_{\bar{n}}$ remains unchanged, as shown in Fig. 6. The turning radius, R, can thus be expressed as,

$$R = \frac{r_{\bar{n}}}{\sin\beta} = \frac{r_{\bar{n}}}{\tan\beta\cos\beta} \approx \frac{r_{\bar{n}}}{\tan\beta}, \tag{9}$$

where a small angle approximation is been made. We can further express $\tan\beta$ as a function of k,

$$\tan\beta = \frac{dy}{dx} = \frac{dy}{ds}\frac{ds}{dx} = \frac{1}{m}\frac{dA(n)}{dn}\frac{ds}{dx} = \frac{k}{mJ_0(\bar{\theta})} \tag{10}$$

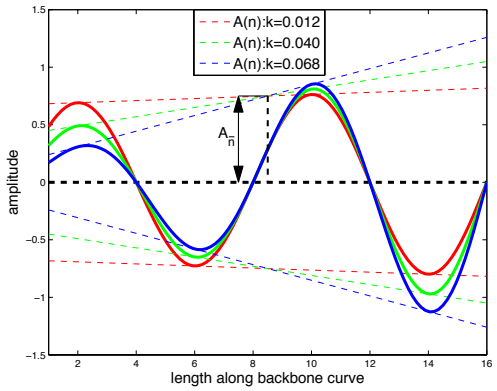

Fig. 9: This figure shows the shapes of *backbone curves* (in different color) with different slope k. Notice that even with different slope k, the amplitude of the serpenoid waves in the middle stays unchanged.

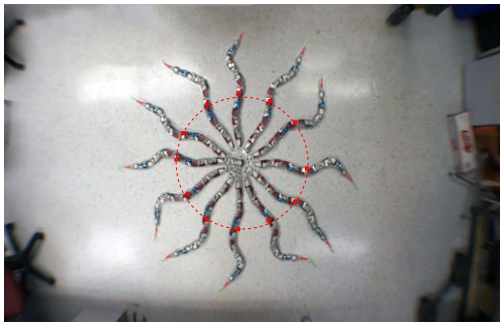

Fig. 10: This image shows a sidewinding snake commanded by our extended gait equation tracing a circular path on the ground. The snake robots showed in the image are fetched from a video stream and stitched together. The red dashed circle is the approximated trace of the COM.

Plugging (10) in (9), we find that,

$$k = mr_{\bar{n}} J_0(\bar{\theta}) \frac{1}{R}. \tag{11}$$

(11) reveals the linear relationship between the slope k in the amplitude function and the reciprocal of turning radius (or turning curvature) of sidewinding.

V. Experiments

Experiments were conducted to corroborate our theoretical results and to evaluate the quality of the turning radius control for sidewinding.

Fifteen total trials of the turning radius experiment were conducted. The slope, k in (11), was varied in the range 0.012 to 0.068, with step size 0.004. In each trial, the snake robot was controlled using the extended gait equation to generate desired joint angles. Video data was recorded during all experimentation. The data was post processed by manually annotating the position of the virtual chassis in individual image frames. The data was then fit using a least squares approximation to retrieve the experimental turning radii, as illustrated in Fig. 10 for one trial.

A. Measurements

Fig. 11 shows an example of a post processed image containing experimental data from 5 trials; markers in different

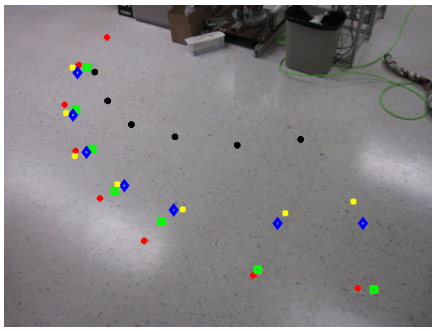

Fig. 11: Raw data of 5 sets of experiments are shown in the above figure. Distinct markers belong to different set. This image suffers a projective distortion which has to be rectified to provide accurate spatial information.

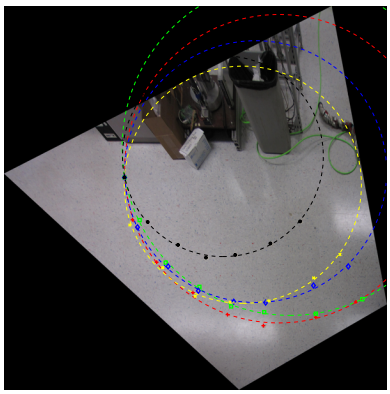

Fig. 12: This is the rectified image of Fig. 11. 5 circles are individually fitted onto each data set, denoted by dashed circles in different colors.

colors denote the origins of the *virtual chassis* belonging to different trials.

In order to capture a wider field of view, the experimental video data was taken from an angle, not perpendicular to the ground. In order for the post-processed image to thus provide meaningful spatial information, the images needed to be transformed into the *correct* view. Knowing the ground is planar and the absolute size of the square ground tile in the space where the experiments were conducted, a homographic transformation to rectify the image was performed. Fig. 12 shows one example of a rectified image. After transforming the images, the marked origins of manually annotated *virtual chassis* frames were fit to circles for each experiment set. The circle fitting was accomplished via a least square approximation, minimizing the fitting error defined as,

$$\mathcal{H}^k = \sum_{i=1}^{N^k} \left((x_i^k - x_r^k)^2 + (y_i^k - y_r^k)^2 - {r_r^k}^2 \right)^2, \tag{12}$$

where (x_i^k, y_i^k) is a position measurement of the experiment set k, N^k is the total number of data points of experiment k and r_r^k is the fitted radius.

B. Data Analysis

In order to prove a basis of comparison with respect to the evolution of turning radius under change of slope, k in (8),

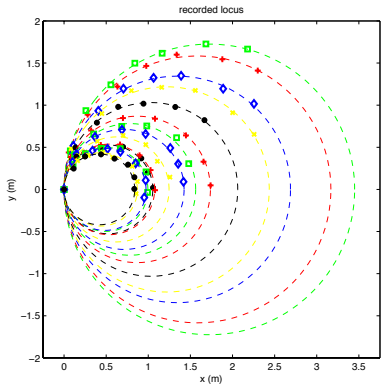

Fig. 13: 15 sets of experimental data are together shown in this figure. Markers of same color and shape are the measured COM positions belonging to the same experiment set. 15 circles are independently fitted onto the data to recover the turning radii of sidewinding.

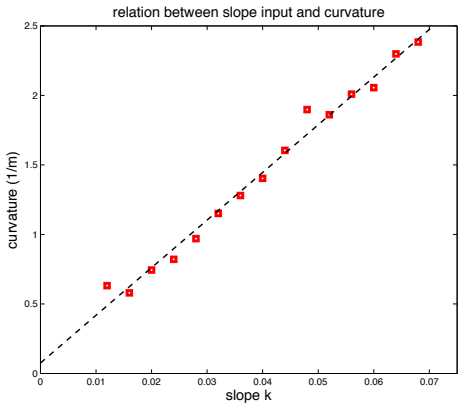

Fig. 14: This figure shows the relation between the slope k and the resulting turning curvature $\frac{1}{R}$. Each of the 15 markers stands for one experiment. The dashed line describes linear relation between k and $\frac{1}{R}$.

the raw measurements and fitted circles were integrated into a single plot, as illustrated in Fig. 13. In general, we observed that with an incremental increase of slope k, the turning radii gradually decrease (turning curvature increases). Theoretically, according to (11), the turning curvature of sidewining should be linearly proportional to the slope k. In Fig. 14, the experimental data is plotted in terms of turning curvature versus input slope k. A linear relationship of the data is indeed observed, and the following relationship is recovered using linear regression

$$\frac{1}{R} = 34.2692k + 0.0753, \tag{13}$$

which is represented by the dashed line in Fig. 14.

The linear relation between $\frac{1}{R}$ and k in (13) demonstrates the consistency between experimental results and analytical derivation in (11). This experimental verification proves that the extended gait equation model, (2), provides precise and intuitive control for the turning radius of the conical sidewinding gait.

VI. Conclusions and Future Work

In this work, we propose a new approach to find an analytical counterpart to the geometric model of a snake gait. Applying this approach to sidewinding, we establish the extended gait equation which eliminates the dependency of conical sidewinding on the computationally expensive *chain fitting* algorithm, and makes real-time, continuously-varying parameterized control possible. This extended gait equation also provides a richer set of controls for the path planning community.

Recent work has shown that the conical sidewinding gait demonstrates somewhat remarkable capabilities for locomoting over rocky terrain. We empirically discovered that by varying the amplitude along the *backbone curve* in specific ways, the robot was able to traverse rubble piles which were previously impassible. This observation raises our interests in developing a more sophisticated amplitude function to explore further capabilities of locomotion in unstructured environments.

Acknowledgments

We would like to acknowledge the assistance of Lu Li with the experimental portion of this work. Grateful acknowledgment is made to Ross L. Hatton for permission to use Fig. 1.

References

[1] M. Tesch, K. Lipkin, I. Brown, R. Hatton, A. Peck, J. Rembisz, and H. Choset, "Parameterized and scripted gaits for modular snake robots," *Advanced Robotics*, vol. 23, no. 9, pp. 1131–1158, 2009.

[2] J. Burdick, J. Radford, and G. Chirikjian, "A "Sidewinding" Locomotion Gait for Hyper-redundant Robots," *Robotics and Automation*, vol. 3, pp. 101–106, 1993.

[3] R. L. Hatton and H. Choset, "Generating gaits for snake robots by annealed chain fitting and keyframe wave extraction," in *Proceedigns of the IEEE/RSJ International Conference on Intelligent Robots and Systems*, St. Louis, MO USA, October 2009.

[4] ——, "Sidewinding on slopes," in *Proceedings of the IEEE International Conference on Robotics and Automation*, Anchorage, AK USA, May 2010, pp. 691–696.

[5] K. Lipkin, I. Brown, A. Peck, H. Choset, J. Rembisz, P. Gianfortoni, and A. Naaktgeboren, "Differentiable and Piecewise Differentiable Gaits for Snake Robots," in *Proceedings of IEEE/RSJ Intl. Conference on Intelligent Robots and Systems*, San Diego, CA, USA, Oct 29 - Nov 2 2007, pp. 1864–1869.

[6] J. Gonzalez-Gomez, H. Zhang, E. Boemo, and J. Zhang, "Locomotion Capabilities of a Modular Robot with Eight Pitch-Yaw-Connecting Modules," in *9th International Conference on Climbing and Walking Robots.*, 2006.

[7] J. Gonzalez-Gomez, H. Zhang, and E. Boemo, "Locomotion Principles of 1D Topology Pitch and Pitch-Yaw-Connecting Modular Robots," in *Bioinspiration and Robotics: Walking and Climbing Robots*. Advanced Robotics Systems International and I-Tech Education and Publishing, 2007.

[8] S. Yu, S. Ma, B. Li, and Y. Wang, "Analysis of Helical Gait of a Snake-like Robot," in *Proceedings of the IEEE/ASME International Conference on Advanced Intelligent Mechatronics*, 2008.

[9] C. Gong, R. Hatton, and H. Choset, "Conical sidewinding," in *Robotics and Automation (ICRA), 2012 IEEE International Conference on*, may 2012, pp. 4222 –4227.

[10] W. Mosauer, "A Note on the Sidewinding Locomotion of Snakes," *The American Naturalist*, vol. 64, no. 691, pp. 179–183, March 1930.

[11] D. Rollinson and H. Choset, "Virtual chassis for snake robots," in *Intelligent Robots and Systems (IROS), 2011 IEEE/RSJ International Conference on*, sept. 2011, pp. 221 –226.

[12] S. Hirose, *Biologically Inspired Robots (Snake-like Locomotor and Manipulator)*. Oxford University Press, 1993.

[13] H. Yamada and S. Hirose, "Approximations to continuous curves of active cord mechanism made of arc-shaped joints or double joints," in *Robotics and Automation (ICRA), 2010 IEEE International Conference on*, may 2010, pp. 703 –708.